# Ultra-Tight GPS/INS for Carrier Phase Positioning in Weak-Signal Environments

**M.G. Petovello, C. O'Driscoll and G. Lachapelle**
Position, Location And Navigation (PLAN) Group
Department of Geomatics Engineering
Schulich School of Engineering
University of Calgary
Calgary, Alberta, Canada
T2N 1N4

[mpetovello, codriscoll, lachapelle]@geomatics.ucalgary.ca

## *ABSTRACT*

*Most high-sensitivity GNSS (HSGNSS) receivers focus on pseudorange measurements, thereby limiting obtainable positioning accuracy to tens of metres. In this paper use of an ultra-tight GPS/INS navigation strategy is proposed for carrier phase based (i.e., centimetre-level) positioning in weak-signal environments.*

*The use of INS-aided tracking loops allows the INS to account for local receiver dynamics, thereby permitting the GPS receiver to narrow the bandwidth of its phase tracking loops. This in turn leads to improved carrier phase tracking at low $C/N_o$. In the ultra-tightly coupled integration strategy the GPS channel estimates of Doppler frequency and code phase are directly updated by the navigation filter, thus permitting the receiver to "coast" through GPS signal outages as the INS tracks local level dynamics. This strategy is equivalent to a vector GPS receiver (augmented by an INS), allowing collaborative tracking of all received satellite signals.*

*In this paper the implementation of a software-based ultra-tight GPS/INS receiver is presented. Results from a pedestrian-based field test are presented and compared for both a standard (scalar) receiver and the ultra-tight GPS/INS receiver. A signal attenuator is applied to all satellite signals simultaneously and the effect on carrier phase positioning is compared for the two receiver types. Results indicate the ultra-tight receiver provides a sensitivity improvement of approximately 7 dB while maintaining centimetre-level accuracy.*

## 1.0 INTRODUCTION

High-sensitivity GNSS (HSGNSS) receivers are capable of providing satellite measurements for signals attenuated by approximately 30 dB [e.g. 1-3]. This capability is impressive and extends positioning capability, and the tactical applications that require position, dramatically. However, the focus of HSGNSS is generally on pseudorange measurements, thus limiting obtainable positioning accuracy to tens of metres.

In contrast, real-time kinematic (RTK) positioning capability (i.e., centimetre-level) in degraded environments has not received as much attention, even though many systems require, or could benefit from, such high positioning accuracy. Some potential benefits of RTK positioning in a tactical environment include precise relative positioning of two (or more) vehicles (e.g., for autonomous vehicle operation), precise relative motion

Petovello, M.G.; O'Driscoll, C.; Lachapelle, G. (2007) Ultra-Tight GPS/INS for Carrier Phase Positioning in Weak-Signal Environments. In *Military Capabilities Enabled by Advances in Navigation Sensors* (pp. 30-1 – 30-18). Meeting Proceedings RTO-MP-SET-104, Paper 30. Neuilly-sur-Seine, France: RTO. Available from: http://www.rto.nato.int.

over time (e.g., for system/sensor calibration) and enhanced personal navigation/personnel tracking accuracy. Even if RTK positioning is not possible, the use of a float ambiguity solution (instead of fixed ambiguity solution with RTK) would provide tremendous improvements over pseudorange-based algorithms; primarily in terms of multipath mitigation. Unfortunately, tracking requirements for the carrier phase are much more stringent than those for pseudorange or carrier frequency, and loss of carrier lock is likely when the received GNSS signals are weaker than normal. As such, RTK positioning is generally reserved for environments where the GNSS signals received at the user's antenna have minimal attenuation.

The idea of using an inertial navigation system (INS) to improve GNSS signal tracking using an ultra-tight, or deep, integration strategy has been proposed and studied by several authors [4-17]. The basic tenet of ultra-tight integration is that the INS can remove most of dynamics from the incoming signal, allowing for a tightening of the signal tracking loops and a commensurate improvement in noise mitigation. However, only a few studies [1, 4, 12, 14-17] focus on the carrier phase measurement and/or RTK positioning. Fewer still focus on carrier phase tracking in weak signal conditions. Rather, most studies are more focused on the code phase (pseudorange) and/or Doppler measurements and/or carrier phase tracking during high-dynamics or in the presence of jamming. Although analysis of frequency (Doppler) tracking provides an insight into carrier phase tracking performance [8, 9, 13], a confident extrapolation of these results to the carrier phase/RTK domain is not possible.

In this paper the implementation of a software-based ultra-tight GPS receiver is presented. Field data results are included to illustrate performance, primarily in terms of carrier phase tracking and RTK positioning capability. The major objective of the paper is to help understand the expected improvement in terms of carrier phase tracking performance and RTK accuracy of an ultra-tight receiver relative to traditional receiver architectures. As such, coherent integration times of only 20 ms are considered in both cases, with the expectation that that same level of improvement (or more) will be possible as integration times are extended.

A pedestrian-based field test was performed using a tactical-grade inertial measurement unit (IMU) in a relatively benign signal environment. A variable signal attenuator was also used in order to have control over the signal levels received, thus facilitating data analysis. When all satellites in view are attenuated simultaneously, results indicate that the ultra-tight receiver architecture provides roughly 7 dB of carrier phase tracking improvement over traditional architectures and therefore represents a significant improvement.

The paper begins with a brief overview of the traditional and ultra-tight receiver architectures, including a discussion on their relative merits and drawbacks. Second, the pedestrian-based field test and the equipment used are described. The results of data processing and analysis are then presented with emphasis given to the carrier phase and RTK performance. Finally, results are summarized and conclusions are drawn.

## 2.0 METHODOLOGY

In terms of tracking, the basic objective any GNSS receiver is to generate a local signal that most accurately matches the one being received. In standard receiver architectures, this is done on a satellite-by-satellite basis (one satellite per channel) with no information being shared or communicated between tracking channels. This approach is therefore sometimes called "scalar tracking". However, because all of the signals are being received by a common antenna they are related to each other via the position. Vector-tracking receivers aim to observe the position and velocity of the antenna directly in an attempt to improve signal tracking [18-21]. Ultra-tightly integrated GNSS/INS receivers are, in many ways, an extension of vector-tracking wherein an INS is used to improve positioning capability.

Standard (scalar), vector and ultra-tight receiver architectures are presented in the following sections along with a brief discussion of their relative merits and drawbacks.

## 2.1 Standard Tracking

The standard, scalar-tracking, receiver architecture is shown in Figure 1. Down-converted and filtered samples are passed to each channel in parallel. The samples are then passed to a signal processing function where Doppler removal (baseband mixing) and correlation (de-spreading) is performed. The correlator outputs are then passed to an error determination function consisting of discriminators (typically one for code, frequency and phase) and loop filters. Finally, the local signal generators — whose output is used during Doppler removal and correlation — are updated. As necessary/requested, each channels' measurements are incorporated into the navigation filter to estimate position, velocity and time parameters.

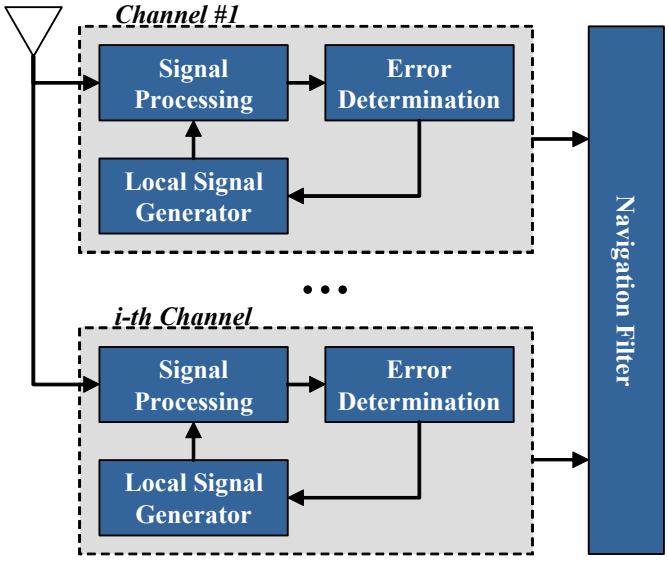


**Figure 1 - Standard Receiver Architecture**

The benefits of scalar-tracking are the relative ease of implementation and a level of robustness that is gained by not having one tracking channel corrupt another tracking channel. However, on the downside, the fact that the signals are inherently related via the receiver's position and velocity is completely ignored. Furthermore, the possibility for one tracking channel to aid another channels is impossible. For more information on scalar-tracking, please refer to [20, 22-24].

## 2.2 Vector Tracking

In contrast to scalar-tracking, vector-tracking estimates the position and velocity of the receiver directly. A basic vector-tracking architecture is shown in Figure 2. As can be seen, the individual tracking loops are eliminated and are effectively replaced by the navigation filter. With the position and velocity of the receiver known, the feedback to the local signal generators is obtained from the computed range and range rate to each satellite.

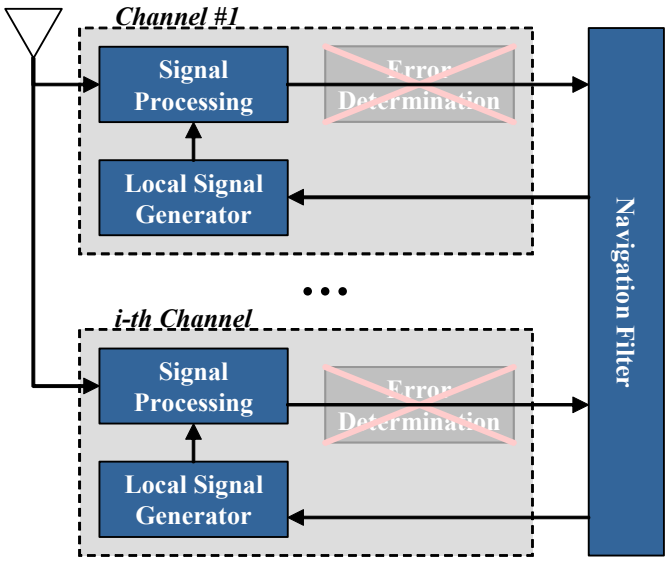


**Figure 2 - Vector-Tracking Receiver Architecture**

The primary advantages of vector-tracking are [20]; noise is reduced in all channels making them less likely to enter the non-linear tracking regions; it can operate with momentary blockage of one or more satellites; and it can be better optimized than scalar-tracking approaches. Vector-tracking is also able to improve tracking in weak-signal or jamming environments, especially when integrated with inertial sensors [7, 12, 18]. The primary drawback is that all satellites are intimately related, and any error in one channel can potentially adversely affect other channels.

## 2.3 Ultra-Tight Tracking

The ultra-tight integrated receiver architecture is similar to that of the vector-based receiver shown in Figure 2. The difference is the inclusion of an IMU and a set of mechanization equations. The navigation filter is also updated to include the inertial error states, as necessary.

It is also noted that, for efficiency, many studies use a federated or cascaded approach to implement the vector-based or ultra-tight receiver architectures [8, 9, 12, 19, 25]. In this case, each channel has an associated local filter that estimates the tracking errors for that channel. This is illustrated in Figure 3 for the ultra-tight receiver architecture. The advantage of this is two fold. First, depending on the implementation of the navigation filter, it can reduce the order of the navigation filter state vector. Second, the output from the local filter can be sent to the navigation filter at a lower rate, thus improving efficiency. It is noted that in Figure 3, feedback can optionally be made directly from the local filter to the local signal generator. This applies primarily to the carrier phase, since the navigation solution accuracy (or more correctly, the temporal variability of the navigation solution) is insufficient for carrier phase tracking.

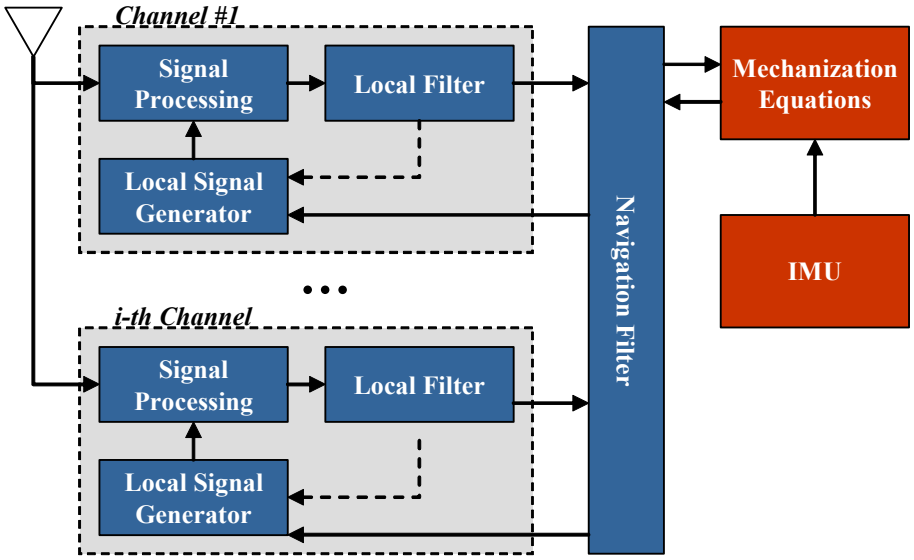


**Figure 3 - Ultra-Tight Receiver Architecture with Cascaded Filters**

The structure of the local filters can take any suitable form, as for example, in [19, 25-19]. For this paper, option #1 from [19] is adopted because it provides reasonable results and is relatively easy to implement.

The drawbacks of the ultra-tight receiver are the same as those listed for the vector-based receiver. In terms of benefits however, the ultra-tight receiver should outperform the vector-based receiver because the inertial sensors can measure the actual antenna motion between navigation filter updates whereas the vector receiver would have to predict the navigation solution forward with relatively more error. This is particularly important when coherently integrating over longer time intervals where predicting the navigation solution may introduce additional attenuation.

It should be noted that the inertial sensors are only able to compensate for changes in the antenna-to-satellite geometry; including lever-arm effects between the IMU and GPS antenna and phase wind-up effects. In other words, it provides no benefit if the received signal varies because of "non-geometric" effects such as receiver clock errors, multipath or interference. Although this would seem to be a positive effect, care should be exercised since it has been observed that, in some instances, this can generate measurement biases in the carrier phase, as will be shown later.

## 2.4 Software Implementation

The above three receiver architectures have been implemented in different versions of the University of Calgary's GSNRx™ (GNSS Software Navigation Receiver) software suite. The software is configurable to select the maximum coherent integration time, tracking loop filter parameters, the type of navigation solution (least squares or Kalman filter), etc. The source code is modular to allow extensive code re-use; an important consideration given the comparisons to be made later.

The software is currently configured to acquire and track GPS L1 C/A code only. For the ultra-tight case (GSNRx-ut™), the receiver was initialized using scalar tracking. Once the receiver was able to extract system time and a valid ephemeris, it switched to ultra-tight mode. For the ultra-tight implementation, the INS

mechanization equations were implemented in the local-level frame [30]. The Kalman filter estimated the position, velocity and attitude errors as well as the IMU gyro and accelerometer biases. The latter were modelled as first order Gauss-Markov processes (e.g., as in [31]).

# 3.0 DATA COLLECTION

Live GPS data was collected using a pedestrian-based system in order to assess the performance of the system. The following sections described the setup in more detail.

## 3.1 Equipment

A schematic of the system setup is shown in Figure 4 and pictures are shown in Figure 5. The data was collected in an open sky environment with a few nearby multipath sources. In order to decrease the received signal power, a variable attenuator with a range of 0-60 dB was inserted prior to the front-end, which in this case consisted of a NovAtel Euro 3M receiver outputting complex samples at 20 MHz. The complex samples are then passed to an FPGA (Field Programmable Gate Array) that restructures the data for compactness before forwarding them to the PC via a National Instruments data acquisition card. The samples are stored on the PC and can be processed in post-mission using the GSNRx™ software.

The rover equipment consisted of a test antenna, as well as a NovAtel SPAN™ (Synchronized Position Attitude Navigation) system [32]. The SPAN™ system consists of a NovAtel OEM4 receiver and an IMU; in this case a Honeywell HG1700AG11 (“HG1700”). The HG1700 is a tactical-grade IMU with specifications listed in Table 1 [33]. Raw GPS measurements were logged at 1 Hz and raw IMU data was logged at 100 Hz. The role of the SPAN™ system is two-fold. First, the inertial data is time tagged and can therefore be more easily integrated into the ultra-tight receiver software. Second, because the SPAN antenna is not affected by the variable attenuator, it is able to track all satellites in view and provide high quality carrier phase data therefrom. This data, in turn, is used to generate a reference solution. Data from a MEMS-grade Crista IMU was also collected, but those were not processed herein.

The NovAtel Euro 3M receiver was driven by an external oscillator; in this case a Symmetricom 1000B OCXO. This oscillator is very stable over time intervals of several seconds and has been shown to allow coherent integration of up to 15 s with only about 1 dB worth of attenuation due to phase and frequency errors [34]. Such an oscillator is currently unfeasible for mass-deployment due to its high cost. It was included during testing to better assess the best possible performance of an ultra-tight receiver. The results presented below should therefore be considered in this light. Ultimately, the performance (and thus benefit) of the ultra-tight receiver for weak-signal tracking will also be influenced by the oscillator [34].

In addition to the rover equipment, a NovAtel OEM4 receiver was setup on a nearby pillar with accurately determined coordinates to act as a base station. The receiver’s raw GPS measurements were logged to file and were used for RTK processing. The base station data logging PC was also used to control the variable attenuator. The base station receiver maintains accurate time throughout the test (i.e., not affected by the attenuator) and was therefore used to time tag the changes in the attenuator levels.

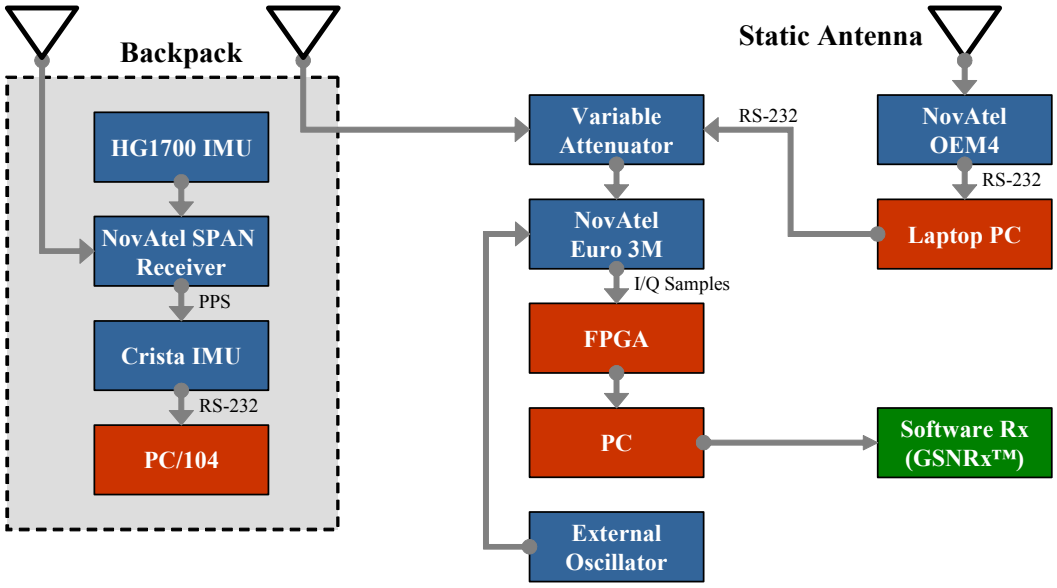


Figure 4 - Schematic of Test Setup

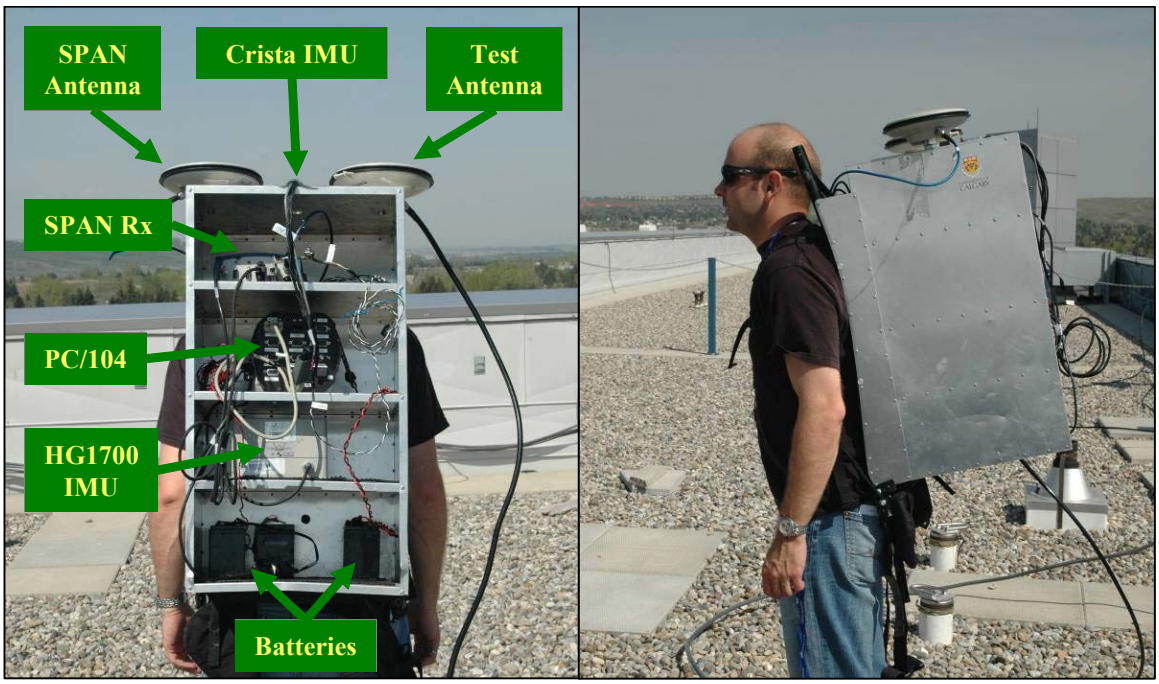


Figure 5 - Picture of Test Setup

Table 1 - Honeywell HG1700AG11 Specifications [33]

| Parameter | Specified Value | |
|---|---|---|
| | Gyro | Accelerometer |
| Bias (1σ) | 1 deg/h | 1 milli-G |
| Scale Factor (1σ) | 150 ppm | 300 ppm |
| Misalignment (1σ) | 500 μrad | 500 μrad |

## 3.2 Test Description

In total, the test lasted just over 14 minutes and seven satellites were in view. The rover was initialized in a static position for approximately 4.25 min. The initialization was performed without any signal attenuation (i.e., attenuation of 0 dB) to allow sufficient time for the software receiver to acquire all available satellites and their ephemerides. More importantly however, the initialization provides a time period during which the ambiguities can be reliably fixed to integers prior to motion.

Following the initialization, and with the attenuator still set at 0 dB, the system was carried in a rectangular pattern spanning roughly 8 m north/south and 3 m east/west. The rectangular pattern was traversed in both clockwise and counter-clockwise directions. After approximately 4.5 min of walking, the signals were attenuated at a rate of 1 dB every four seconds until a maximum attenuation of 60 dB was reached. The same rectangular walking pattern was maintained during the attenuation phase of the test.

The maximum speed of the antenna during the test was just below 1.6 m/s. However, the acceleration had a peak-to-peak range of about 10 $m/s^2$ in each coordinate direction. Furthermore, because this acceleration was induced mostly from the walking motion (and less so from the actual trajectory), it is periodic throughout the data set with a period of roughly 2 Hz.

## 3.3 Data Processing

As mentioned before, the complex samples were processed using the University of Calgary's GSNRx™ software suite. To reduce processing time, the data were down-sampled from 20 MHz to 5 MHz. For the standard receiver (GSNRx™) an FLL-assisted-PLL was used for carrier tracking. Relevant receiver settings are summarized in Table 2. The raw pseudorange, Doppler and carrier phase measurements were output to file at a rate of 20 Hz.

The output from each software receiver was then processed using the University of Calgary's FLYKIN+™ processing software (as described in [35]). FLYKIN+™ uses double difference processing and on-the-fly carrier phase ambiguity resolution to obtain centimetre-level positioning accuracies. The software was configured to process L1-only GPS data and to wait 60 seconds before trying to resolve the ambiguities. Unfortunately, the data from the base station was logged at 1 Hz, instead of at 20 Hz. Although this poses no significant problem (it merely limits the RTK output rate), it means that fewer solutions are available at each attenuation level (see below).

**Table 2 - Software Receiver Settings**

| Parameter | Standard Receiver | Ultra-Tight Receiver |
|---|---|---|
| Maximum Coherent Integration | 20 ms | |
| Carrier-Aided DLL Loop Bandwidth | 0.05 Hz | N/A |
| FLL Loop Bandwidth | 8 Hz | N/A |
| PLL Loop Bandwidth | 5 Hz | N/A |
| Navigation Solution | Kalman Filter (random walk velocity) | Kalman Filter (INS) |
| Measurement Output | 20 Hz | |

The reference solution was obtained using the University of Calgary's SAINT™ (Satellite And Inertial Navigation Technology) software (as described in [31, 36]). The SAINT™ software processes GPS and IMU data and is able to resolve the carrier phase ambiguities on-the-fly. For the current tests, the GPS data logged by the SPAN™ receiver was used to generate the reference solution because it is not affected by the signal attenuator and because it is independent of the data generated by the GSNRx™ software. The solution was then translated to the second antenna using the measured lever-arm (roughly 0.5 m long) and the estimated INS attitude. The carrier phase ambiguities were resolved prior to, and remained fixed throughout, the kinematic portion of the test. The accuracy of the solution is on the order of 1-2 cm.

## 4.0 PERFORMANCE ANALYSIS

The carrier to noise-density ratio ($C/N_o$) estimated from the ultra-tight receiver and the attenuation level are shown in Figure 6. Results from the standard receiver are virtually identical and are therefore not shown. During the static initialization (up to about 414944 s) the $C/N_o$ values are approximately constant. Once motion begins, the $C/N_o$ values show considerably more variation. The periodic variation is caused by the vertical gain pattern of the antenna and the fact that the antennas are pitched forward by roughly ten degrees (see the right picture in Figure 5). The forward pitch means that the elevation angle of the received signal *seen by the antenna* changes by up to 20 degrees as the pedestrian moves towards or away from a particular satellite. This is seen in Figure 6, where the periodic variation of the $C/N_o$ is consistent with the period of the rectangular trajectory (and is asynchronous between satellites because of their distribution in the sky).

Starting at 414210 s, the attenuation was increased by 1 dB every four seconds. The estimated $C/N_o$ decreases at approximately the same rate. Although the attenuation was eventually increased to 60 dB, the results here are limited to 30 dB or less because the receivers could not track beyond this point (due to the relatively short coherent integration time used).

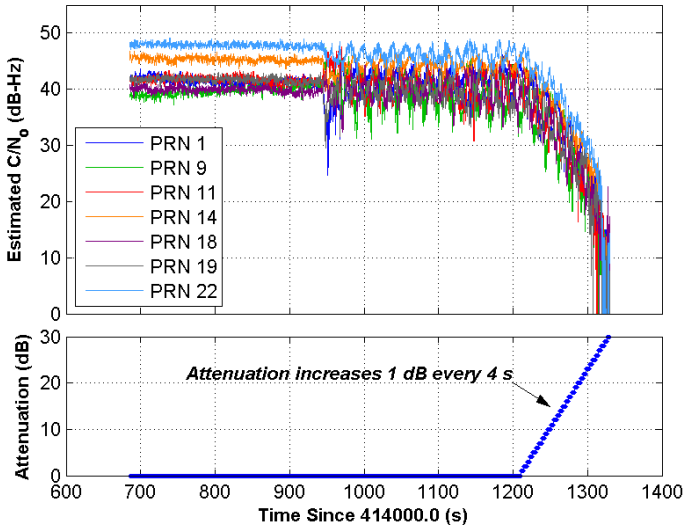


**Figure 6 - Estimated Carrier-to-Noise Density ($C/N_o$) from Ultra-Tight Receiver and Level of Attenuation versus Time**

The following sections present, compare and analyze the performance of the two receivers in terms of their raw measurements, their ability to maintain fixed ambiguities and the resulting position accuracy.

## 4.1 Measurement Comparison

As a first step to comparing the standard and ultra-tight implementations, the raw measurements from the two receivers were differenced. Such an approach allows for identification of any abnormal or unexpected behaviour. Furthermore, because the RTK solutions are derived from the raw data, comparing the data from the two receivers may help in further analysis.

The pseudorange differences are shown in Figure 7. The differences are only shown for the period prior to activating the attenuator because, beyond that point, the comparison is complicated by the increased level of noise. As shown, the errors are initially large until the local filters converge after a few seconds. After convergence however, the differences are generally less than about 2 m and show relatively slow variations (periods on the order of seconds).

Due to its cooperative tracking nature, it is expected that the ultra-tight receiver would generate more accurate pseudorange measurements than would the standard receiver [20]. To confirm this, the data from each software receiver was processed with the University of Calgary's $C^3NAVG^{2}$™ software, which computes an epoch-by-epoch least-squares position solution. The standard deviation of the pseudorange residuals are shown in Table 3. Generally, the ultra-tight receiver has better statistics. In particular, PRNs 1 and 9 (the two satellites showing the largest errors in Figure 7) show an improvement of about 0.16 m and 0.23 m respectively.

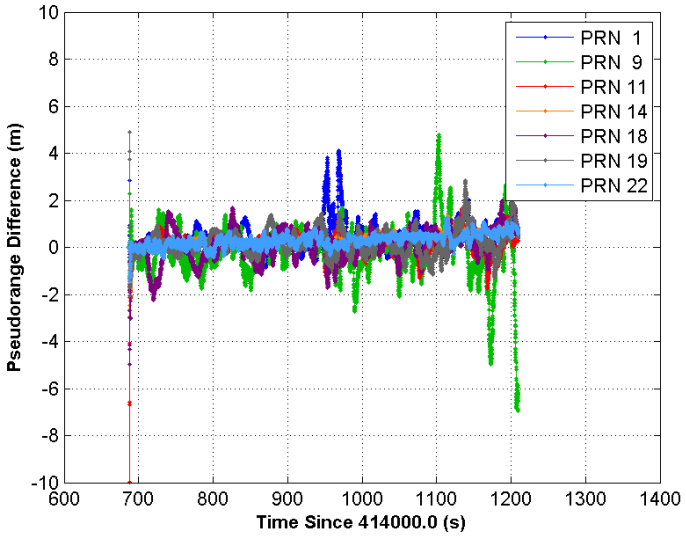


**Figure 7 - Difference in Measured Pseudorange from Standard and Ultra-Tight Receivers**

**Table 3 - Least-Squares Pseudorange Residuals Standard Deviations for Standard and Ultra-Tight Receiver during Strong Signal Conditions**

| PRN | Standard Deviation (m) | |
|---|---|---|
| | Standard | Ultra-Tight |
| 1 | 0.57 | 0.41 |
| 9 | 0.60 | 0.37 |
| 11 | 0.51 | 0.34 |
| 14 | 0.32 | 0.33 |
| 18 | 0.54 | 0.36 |
| 19 | 0.71 | 0.55 |
| 22 | 0.37 | 0.38 |

Differences in the measured carrier phase data are shown in Figure 8. There are two marked differences relative to the pseudorange results. First, there is no convergence time because the estimated carrier phase error in the local filters is highly observable and is fed directly to the local carrier phase generator (see Figure 3). Second, and more importantly, there are carrier phase biases that are the result of cycle slips. Furthermore, in some cases, the cycle slips are actually half-cycle slips (a good example is the first slip on

PRN 1 at about 414950 s). Not every (half-)cycle slip was investigated in detail, but it is noted that in some cases a slip occurred with the ultra-tight receiver and not with the standard receiver. This is unexpected and is being investigated further. Despite this however, the receivers are (after preamble detection) able to correct for the half-cycle slips. The full cycles are detected and handled by the FLYKIN+™ software, as will be evident when assessing the RTK positioning accuracy below.

Aside from the cycle slips, the two receiver architectures generate phase measurements that differ from each other with a standard deviation of about by less than about 0.02 cycles (less than 4 mm at L1).

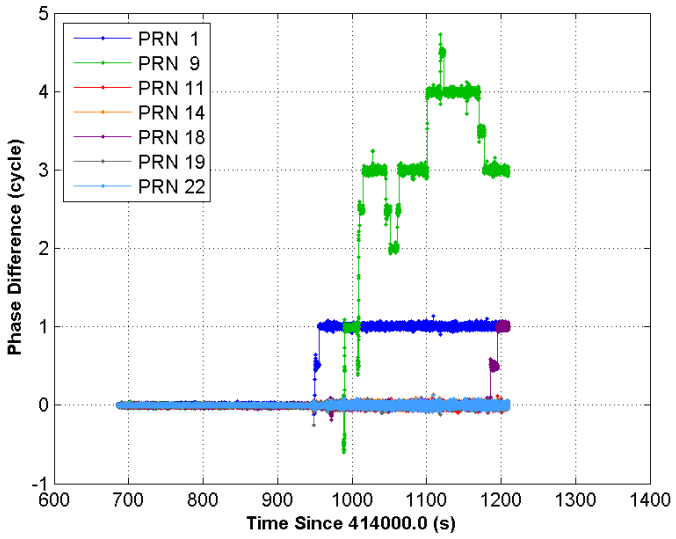


**Figure 8 - Difference in Measured Carrier Phase from Standard and Ultra-Tight Receivers**

## 4.2 Ambiguity Status

Analysis from the previous section suggests that, all things being equal, the standard and ultra-tight receivers should provide similar RTK capability. However, as is well known, the highest positioning accuracy is obtained when the carrier phase ambiguities are fixed as integers. To this end, Figure 9 shows the number of ambiguities that were fixed during FLYKIN+™ processing; on the left the results for the entire test and on the right the results during signal attenuation. Prior to activating the attenuator (at 415210 s), both receivers had all six ambiguities resolved as integers most of the time although sporadic losses of a satellite occurred in both cases due to cycle slips and/or loss of synchronization with the received navigation message.

After the attenuator is activated however, stark differences are seen. Take for example, the time at which each receiver has fewer than six fixed ambiguities. This occurs at time 415259 s and 415302 s for the standard and ultra-tight receivers respectively. Recalling that the attenuation is 1 dB every 4 s, this represents an improvement of approximately 10-11 dB. Similarly, if we consider the times at which each receiver is unable to maintain 3 or more ambiguities (the minimum number to compute a 3D position), the improvement of the ultra-tight receiver is about 10 dB.

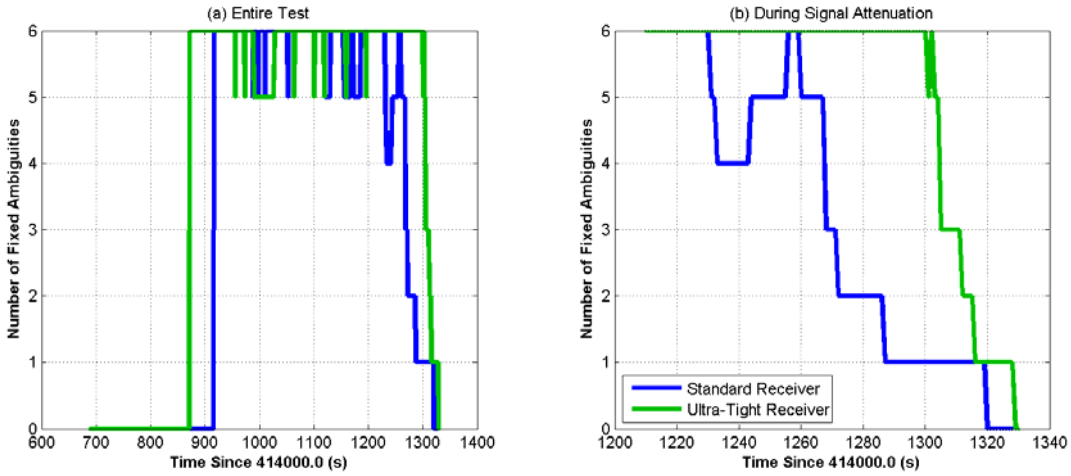


**Figure 9 - Number of Fixed Ambiguities Using Standard and Ultra-Tight Receivers**

## 4.3 Positioning Accuracy

Although the ambiguities are fixed as integers more often in the ultra-tight case, such an improvement is only useful if the ambiguities are correctly determined, thus providing accurate position estimates. Figure 10 shows the position errors for each receiver as a function of signal attenuation. Although the vertical scale is relatively large, the standard receiver clearly shows a more rapid degradation than does the ultra-tight receiver.

To get a better understanding for how the position degrades, Figure 11 shows a histogram for the horizontal position error as a function of maximum attenuation. Results are only plotted for the time period during which the attenuator was activated (before activation, position errors are always less than the lowest threshold for both receivers). The plot shows the number of epochs whose horizontal error exceeds a given threshold for all attenuation values less than the maximum. For example, for epochs with an attenuation of 26 dB or less, the standard receiver has about 45 epochs where the horizontal error exceeds 0.1 m. In contrast, for the same level of attenuation, the ultra-tight receiver has only about 11 epochs where the horizontal error exceeds 0.1 m. An alternative analysis is, for the data analyzed herein, if a horizontal position error of better than 0.1 m is required, the standard receiver can tolerate no more than 14 dB of attenuation. For the same level of accuracy, the ultra-tight receiver can tolerate no more than 22 dB of attenuation. This represents a sensitivity improvement of 8 dB. Overall, for the different horizontal positioning thresholds, the ultra-tight receiver provides between 5 and 8 dB (average of about 7 dB) of sensitivity improvement over the standard receiver.

A histogram of the vertical errors is shown in Figure 12. Improvements range from 4 to 9 dB, depending on the error threshold. As with the horizontal errors, the average sensitivity improvement is about 7 dB.

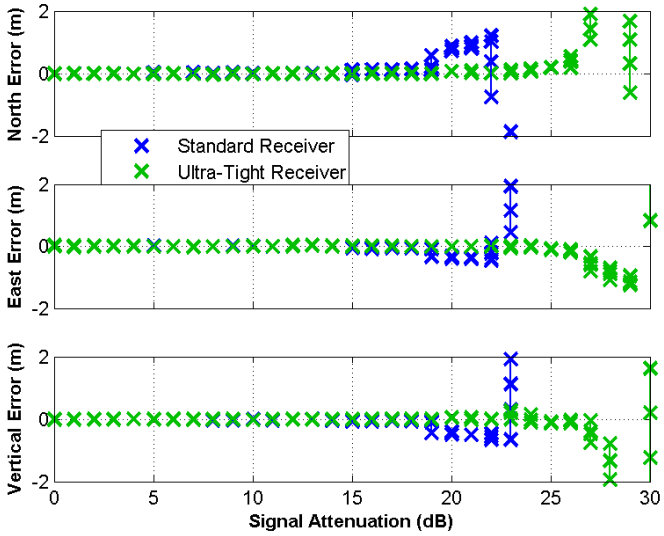


**Figure 10 - Position Error as a Function of Attenuation for Standard and Ultra-Tight Receiver**

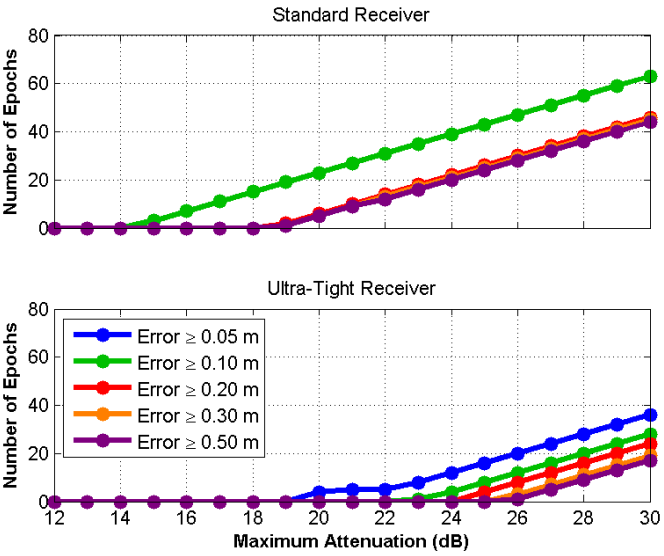


**Figure 11 - Horizontal Position Histogram for Standard and Ultra-Tight Receivers as Computed During Signal Attenuation (lines are plotted in order of increasing error and thus histograms for larger error results may hide smaller error results)**

It is noted that the results presented are based on one set of data and should not be extrapolated to other cases. That said, the ultra-tight receiver architecture is expected to continue to outperform the standard approach in other situations. This is particularly expected in situations where there may be a few strong signals and a few weak signals. This contrasts with the current results which looked at the case where all satellite signals were attenuated simultaneously.

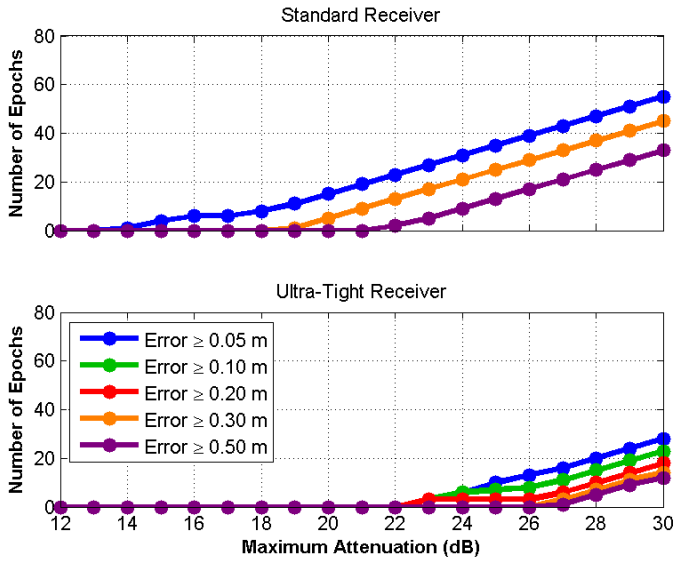


**Figure 12 - Vertical Position Histogram for Standard and Ultra-Tight Receivers as Computed During Signal Attenuation (lines are plotted in order of increasing error and thus histograms for larger error results may hide smaller error results)**

## 5.0 CONCLUSIONS AND FUTURE WORK

This paper investigated the benefit of an ultra-tight GPS/INS receiver architecture for carrier phase positioning in weak signal conditions relative to a standard (scalar-tracking) architecture. A very high accuracy oscillator was used to minimize the effect of oscillator effects and a tactical-grade IMU (1 deg/h) was used for the ultra-tight integration. A pedestrian test was performed and a variable signal attenuator was used to decrease signal power in a controlled manner. All satellite signals were attenuated simultaneously and, in this respect, the test represents a pessimistic situation.

The pseudorange and carrier observations from the standard and ultra-tight receivers were compared. The pseudorange measurements typically agreed to within about 1 m. An analysis of the least-squares pseudorange residuals showed the ultra-tight receiver provides temporally smoother measurements. In terms of the carrier phase, aside from cycle slips, the two receivers produced measurements that agreed to about 1 cm (at L1). Half-cycle differences were observed between the two receivers. Cycle slips occurred with both receivers, although not necessarily at the same time.

Processing the observations with RTK software showed the ultra-tight receiver provided about a 10 dB sensitivity improvement in terms maintaining fixed ambiguities. However, in terms of positioning accuracy, the improvements were observed to range between 4 and 9 dB, with an average of about 7 dB. This represents a significant sensitivity improvement, suggesting that RTK capability could be expanded in some applications.

The results presented were based on a single test conducted in a relatively benign multipath environment. Further tests will be conducted to evaluate performance under more realistic conditions. Results from these tests will be compared and contrasted with those presented here. It is expected that if there are combination of

strong and weak signals, the ultra-tight approach will provide better performance than when all signals are attenuated simultaneously. Lower quality IMUs and longer integration times will also be considered.

## 6.0 ACKNOWLEDGEMENTS

The authors would like to kindly acknowledge and thank Defence Research and Development Canada (DRDC) for funding of this work.

## 7.0 REFERENCES

[1] Fastrax, "iTrax300 OEM GPS Receiver Module," Product Brochure, Fastrax Ltd. 2007. Retrieved July 30, 2007, from http://www.fastrax.fi/showfile.cfm?guid=3fe7f5c9-6a99-4afc-8dc3-0b1ed4fc4df3.

[2] SiRF, "SiRFstarIII GSC3e/LP & GSC3f/LP," Product Brochure, SiRF Technology, Inc. 2007. Retrieved July 30, 2007, from http://www.sirf.com/products/GSC3LPProductInsert.pdf.

[3] ublox, "UBX-G5010, UBX-G5000," Product Brochure, ublox ag. 2007. Retrieved July 30, 2007, from http://www.u-blox.com/products/Product_Summaries/UBX-G5010_Prod_Summary(GPS.G5-X-06042).pdf.

[4] S. Alban, D. Akos, S. M. Rock, and D. Gebre-Egziabher, "Performance Analysis and Architectures for INS-Aided GPS Tracking Loops," in ION National Technical Meeting Anaheim, CA: Institute of Navigation, 2003, pp. 611-622.

[5] D. Gebre-Egziabher, A. Razavi, P. Enge, J. Gautier, S. Pullen, B. S. Pervan, and D. Akos, "Sensitivity and Performance Analysis of Doppler-Aided GPS Carrier-Tracking Loops," NAVIGATION, vol. 52, pp. 49-60, 2005.

[6] D. Gustafson and J. Dowdle, "Deeply Integrated Code Tracking: Comparative Performance Analysis," in ION GPS/GNSS 2003, Portland, OR, 2003, pp. 2553-2561.

[7] D. Gustafson, J. Dowdle, and K. Flueckiger, "A Deeply Integrated Adaptive GPS-Based Navigator with Extended Range Code Tracking," in IEEE PLANS, San Diego, CA, 2000, pp. 118-124.

[8] A. Jovancevic, A. Brown, S. Ganguly, J. Noronha, and B. Sirpatil, "Ultra Tight Coupling Implementation Using Real Time Software Receiver," in ION GNSS 2004, Long Beach, CA, 2004, pp. 1575-1586.

[9] H. S. Kim, S. C. Bu, G. I. Jee, and C. G. Park, "An Ultra-Tightly Coupled GPS/INS Integration Using Federated Filtering," in ION GPS/GNSS 2003, Portland, OR, 2003, pp. 2878-2885.

[10] C. Kreye, B. Eissfeller, and J. O. Winkle, "Improvements of GNSS Receiver Performance Using Deeply Coupled INS Measurements," in ION GPS 2000, Salt Lake City, UT, 2000, pp. 844-854.

[11] D. Landis, T. Thorvaldsen, B. Fink, P. Sherman, and S. Holmes, "A Deep Integration Estimator for Urban Ground Navigation," in ION Annual Meeting/IEEE PLANS, San Diego, CA, 2006, pp. 927-932.

[12] E. J. Ohlmeyer, "Analysis of an Ultra-Tightly Coupled GPS/INS System in Jamming," in ION Annual Meeting/IEEE PLANS, San Diego, CA, 2006, pp. 44-53.

[13] T. Pany, R. Kaniuth, and B. Eissfeller, "Deep Integration of Navigation Solution and Signal Processing," in ION GNSS 2005, Long Beach, CA, 2005, pp. 1095-1102.

[14] J. Sennott and D. Senffner, "Robustness of Tight Coupled Integrations for Real-Time Centimeter GPS Positioning," in ION GPS 1997, Kansas City, MO, 1997, pp. 655-663.

[15] J. Sennott and D. Senffner, "A GPS Carrier Phase Processor for Real-Time High Dynamics Tracking," in ION Annual Meeting, 1997, pp. 299-308.

[16] A. Soloviev, S. Gunawardena, and F. Van Grass, "Deeply Integrated GPS/Low-Cost IMU for Low CNR Signal Processing: Flight Test Results and Real Time Implementation," in ION GNSS 2004, Long Beach, CA, 2004, pp. 1598-1608.

[17] A. Soloviev, F. van Grass, and S. Gunawardena, "Implementation of Deeply Integrated GPS/Low-Cost IMU for Reacquisition and Tracking of Low CNR GPS Signals," in ION National Technical Meeting, San Diego, CA, 2004, pp. 923-935.

[18] T. Pany and B. Eissfeller, "Use of a Vector Delay Lock Loop Receiver for GNSS Signal Power Analysis in Bad Signal Conditions," in ION Annual Meeting/IEEE PLANS, San Diego, CA, 2006, pp. 893-902.

[19] M. G. Petovello and G. Lachapelle, "Comparison of Vector-Based Software Receiver Implementations with Application to Ultra-Tight GPS/INS Integration," in ION GNSS 2006, Fort Worth, TX, 2006, pp. 1790-1799.

[20] J. J. Spilker, Jr., "Fundamentals of Signal Tracking Theory," in Global Positioning System: Theory and Applications. vol. I, B. W. Parkinson and J. J. Spilker, Jr., Eds.: American Institute of Aeronautics and Astronautics, Inc., 1994, pp. 245-327.

[21] M. Lashley and D. M. Bevly, "Analysis of Discriminator Based Vector Tracking Algorithms," in ION National Technical Meeting, San Diego, CA, 2007, pp. 570-576.

[22] P. Misra and P. Enge, Global Positioning System Signals, Measurement, and Performance, 1st ed. Lincoln, MA: Ganga-Jamuna Press, 2001.

[23] A. J. Van Dierendonck, "GPS Receivers," in Global Positioning System: Theory and Applications. vol. I, B. W. Parkinson and J. J. Spilker, Jr., Eds.: American Institute of Aeronautics and Astronautics, Inc., 1995, pp. 329-407.

[24] P. W. Ward, J. W. Betz, and C. J. Hegarty, "Satellite Signal Acquisition, Tracking, and Data Demodulation," in Understanding GPS Principles and Applications, 2nd ed, E. D. Kaplan and C. J. Hegarty, Eds. Norwood, MA: Artech House, Inc., 2006, pp. 153-241.

[25] A. S. Abbott and W. E. Lillo, "Global Positioning Systems and Inertial Measuring Unit Ultratight Coupling Method," United States: The Aerospace Corporation, 2003, p. 22.

[26] G. I. Jee, H. S. Kim, Y. J. Lee, and C. G. Park, "A GPS C/A Code Tracking Loop Based on Extended Kalman Filter with Multipath Mitigation," in ION GPS 2002, Portland, OR, 2002, pp. 446-451.

[27] M. L. Psiaki, "Smoother-Based GPS Signal Tracking in a Software Receiver," in ION GPS 2001, Salt Lake City, UT, 2001, pp. 2900-2913.

[28] M. L. Psiaki and H. Jung, "Extended Kalman Filter Methods for Tracking Weak GPS Signals," in ION GPS 2002, Portland, OR, 2002, pp. 2539-2553.

[29] N. I. Ziedan and J. L. Garrison, "Extended Kalman Filter-Based Tracking of Weak GPS Signals under High Dynamic Conditions," in ION GNSS 2004, Long Beach, CA, 2004, pp. 20-31.

[30] C. Jekeli, Inertial Navigation Systems with Geodetic Applications, 1st ed. Berlin: Walter de Gruyter, 2000.

[31] M. G. Petovello, “Real-Time Integration of a Tactical-Grade IMU and GPS for High-Accuracy Positioning and Navigation,” Geomatics Engineering, University of Calgary, Calgary, 2003.

[32] NovAtel, "SPAN™ Technology," Product Brochure, NovAtel, Inc. 2006. Retrieved August 1, 2006, from http://www.novatel.com/Documents/Papers/SPANTechGuide.pdf.

[33] Honeywell, "Document DS34468-01 - Critical Item Development Specification HG1700AG Inertial Measurement Unit," Honeywell International, Inc., 1997.

[34] R. Watson, M. G. Petovello, G. Lachapelle, and R. Klukas, "Impact of Oscillator Errors on IMU-Aided GPS Tracking Loop Performance," in European Navigation Conference, Geneva, Swizterland, 2007.

[35] J. Liu, M. E. Cannon, P. Alves, M. G. Petovello, G. Lachapelle, G. MacGougan, and L. deGroot, "A Performance Comparison of Single and Dual-Frequency GPS Ambiguity Resolution Strategies," GPS Solutions, vol. 7, pp. 87-100, 2003.

[36] M. G. Petovello, M. E. Cannon, and G. Lachapelle, "Benefits of Using a Tactical Grade INS for High Accuracy Positioning," NAVIGATION, vol. 51, pp. 1-12, 2003.